Macromolecules

pubs.acs.org/Macromolecules Article

Mesoporous Phenolic/POSS Hybrids Induced by Microphase Separation Arising from Competitive Hydrogen Bonding Interactions

Yen-Chi Huang, Wei-Cheng Chen, and Shiao-Wei Kuo*

Cite This: *Macromolecules* 2022, 55, 8918–8930 Read Online

ACCESS | Metrics & More | Article Recommendations | Supporting Information

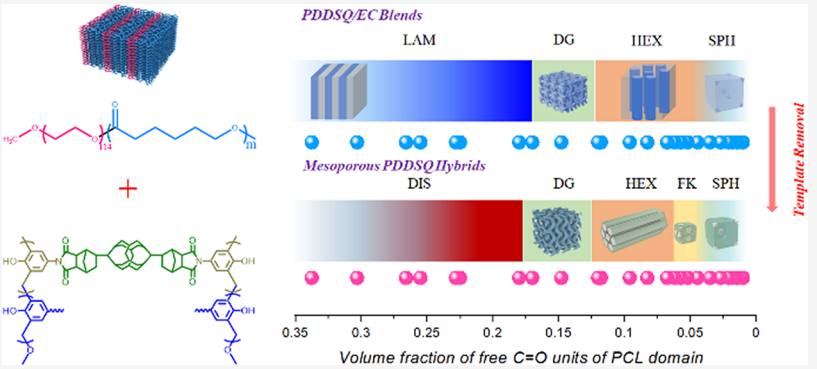

ABSTRACT: We used ring-opening living polymerization to synthesize various linear poly(ethylene oxide−*b*−caprolactone) (PEO-*b*-PCL, EC) diblock copolymers featuring PCL blocks of various molecular weights and prepared phenolic resins with various double-decker silsesquioxane (DDSQ) cage compositions in the form of phenolic/DDSQ (PDDSQ) hybrids. Upon forming PDDSQ/EC blends, competitive hydrogen bonding of the phenolic OH units of PDDSQ occurred with both ether units of the PEO block and C═O units of the PCL block, with the fraction of hydrogen-bonded C═O groups increasing upon increasing the PDDSQ compositions but decreasing upon increasing the molecular weight of the PCL block in EC diblock copolymers. Small-angle X-ray scattering revealed the self-assembled structures and corresponding phase diagram of these PDDSQ/EC blends after thermal polymerization at 150 °C, with the *d*-spacing increasing upon increasing the molecular weight of PCL block in the EC diblock copolymers. After removal of the EC diblock copolymer template, we obtained mesoporous phenolic/DDSQ hybrids possessing high surface areas and pore volumes, with the highly ordered mesoporous structures featuring double-gyroid, hexagonal-packing cylindrical, spherical, and even Frank−Kasper (FK) structures depending on the molecular weight of PCL block and the content of the PPDSQ hybrid. Overall, this study provides a general principle for obtaining mesoporous double-gyroid and FK phases mediated by diblock copolymer compositions through competitive hydrogen-bonding interactions.

INTRODUCTION

The self-assembly of linear diblock copolymers in the bulk state, forming body-centered cubic (BCC), hexagonal-packing cylinder (HEX), double-gyroid (DG), and lamellae (LAM) structures, mediated by the interaction parameter (χ), volume fraction (f), and molecular weight (N), is being investigated widely because of their potential applications in nanopatterns, nanocomposites, drug delivery, and electronic and photonic devices.[1−10] Blending diblock copolymers with homopolymers, copolymers, nanoparticles, and organic−inorganic hybrids to vary the volume fractions and interaction parameters, mediated by hydrogen-bonding interactions, is another simple approach toward fabricating various self-assembled structures.[11−25] Recently, Frank−Kasper (FK) phases, including A15, σ, C14, and C15 phases, have also been observed in the phase diagrams of diblock copolymers through both experimental studies and theoretical predictions.[26−41]

The highly ordered local and complex lattice structures of FK phases were first found in metal alloys; here, the coordination number (CN) should be greater than 12 for at least one polyhedron, while other topologically close-packed polyhedrons should have CNs of 12, 14, 15, or 16.[42−45] Slightly distorted tetrahedra are always observed because regular tetrahedra could not occupy the space completely;

Received: July 31, 2022
Revised: September 14, 2022
Published: September 30, 2022

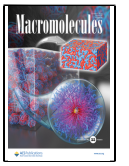

https://doi.org/10.1021/acs.macromol.2c01585
Macromolecules 2022, 55, 8918−8930

Scheme 1. Using (a) EC as Templates in (b) Phenolic/DDSQ Hybrids, with Evaporation Induced Self-Assembly (EISA) and Thermal Curing Leading to (c) PDDSQ/EC Blends, with Subsequent Thermal Calcination Removing the EC Templates and Forming (d) Mesoporous PDDSQ Hybrids

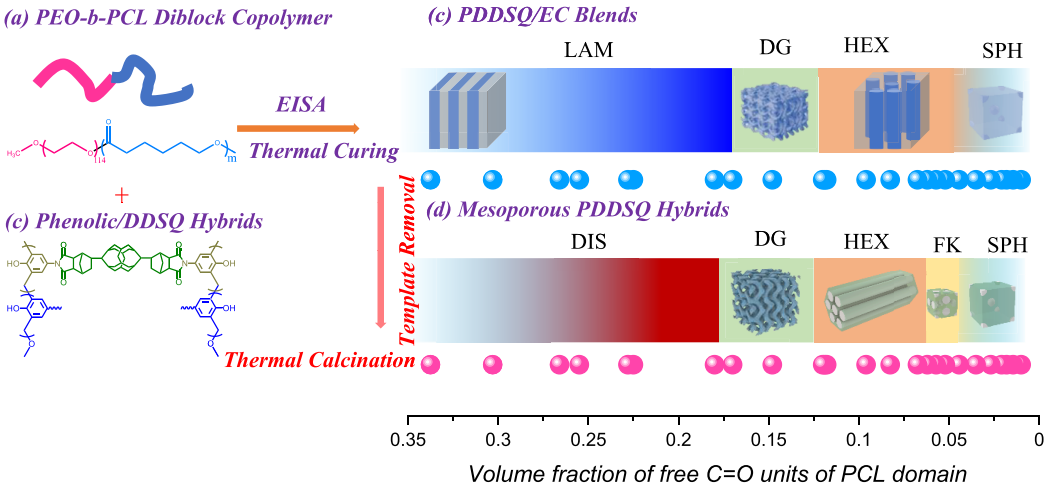

thus, these tetrahedra would be impossible to exist if all of the polyhedra were exactly highly regular.[42−45] The FK phases C14, C15, A15, σ, H, and Z (and 22 others) have been observed experimentally in soft-matter systems, including block copolymers, liquid crystals, dendrimers, and giant amphiphiles based on inorganic polyhedral oligomeric silsesquioxane (POSS) cages or other inorganic nanoparticles.[46−53]

FK σ and A15 phases have appeared in block copolymers with asymmetric compositions, conformations, or architectures; for example, a complex tetrablock copolymer could possibly self-assemble into the A15 phase at a certain temperature or at a small compositional window while heating.[54] Therefore, nonlinear materials, such as star architectures or conformationally asymmetric structures (e.g., ABCA or AB_n materials), were usually found to possess FK phases in earlier studies.[32,55,56] Nevertheless, simple linear diblock copolymers displaying conformational asymmetry with various segment lengths (e.g., linear poly(dodecyl acrylate-*b*-lactide) diblock copolymers) have also been observed to form the σ or A15 phase.[57] Small-angle X-ray scattering (SAXS) and the predictions of self-consistent field theory have revealed that a volume fraction of the lactide block copolymer segment of 0.23−0.25 could possibly form the A15 phase. In addition, blending a homopolymer with a diblock copolymer—for example, poly(1,4-butadiene) with poly(styrene-*b*-1,4-butadiene)—can also result in FK C14, C15, and σ phases. Here, varying the molecular weight of the poly(1,4-butadiene) homopolymer can lead to wet- or dry-brush behavior, thereby optimizing the minimal surface free energy and maxima of the local particle sphericity, resulting in the formation of FK phases; in this case, a higher molecular weight of poly(1,4-butadiene) has led to stronger localization in the spherical region.[38,58] We have proposed that the mesoporous FK phases could also be obtained through the templation of linear PEO-*b*-PCL diblock copolymers into phenolic/double-decker silsesquioxane hybrids (PDDSQ hybrids).[59] Although our group has widely studied the self-assembly of the PEO_{114}-*b*-PCL_{87} (f_{PCL} = 0.67; LAM) diblock copolymer as the template for mesoporous silica, phenolic, and phenolic/silica hybrids, only the HEX and BCC structures have been observed in silica and phenolic/silica hybrids and the DG, HEX, and BCC structures in the phenolic matrices.[23,60−67] As a result, the PDDSQ/EC hybrid system was the first ever found to feature mesoporous FK phases templated by a linear symmetric block copolymer in an organic/inorganic PDDSQ hybrid.[59]

In this present study, we investigated the phase diagram of mesoporous PDDSQ hybrids templated by various PEO-*b*-PCL diblock copolymers to understand the general principles affecting these systems. We used ring-opening living polymerization to prepare various linear PEO-*b*-PCL diblock copolymers featuring different molecular weights of the PCL block and prepared phenolic resins with various DDSQ cage contents in the form of PDDSQ hybrids. Fourier transform infrared (FTIR) spectra and the phase diagram constructed based on small angle X-ray scattering (SAXS) analyses revealed that competitive hydrogen bonding occurred within the PDDSQ/EC blends, with the phenolic OH units of PDDSQ interacting with both ether units of the PEO block and the C═O units of the PCL block. After the removal of the EC diblock copolymer template, we used SAXS, N_2 adsorption/desorption isotherms, and transition electron microscopy (TEM) images to investigate the structures of the resulting self-assembled mesoporous PDDSQ materials. Overall, this study provides a general principle for obtaining mesoporous double-gyroid and FK phases by varying the compositions of a block copolymer and influencing its competitive hydrogen bonding interactions.

EXPERIMENTAL SECTION

Materials. Phenyltrimethoxylsilane, methyldichlorosilane, nadic anhydride, triethylamine, sodium hydroxide (NaOH), Pt(dvs), phenol, 4-aminophenol, charcoal, magnesium sulfate ($MgSO_4$), CH_2O, 2-propanol, tetrahydrofuran, methanol, toluene, dimethylformamide (DMF), acetonitrile, 1,4-dioxane, ethyl acetate (EtOAc), and hydrochloric acid (HCl) were purchased from Acros. PEO-*b*-PCL diblock copolymers (Scheme 1a; ^1H and ^{13}C NMR spectra in Figures S1 and S2) and phenolic/DDSQ hybrids (Scheme 1b; FTIR spectra in Figure S3) were synthesized according to previously reported procedures.[59−68] The molecular weights, polydispersity indices (PDI), and compositions of PEO-*b*-PCL diblock copolymers (abbreviation as EC diblock copolymer; EC1 and EC5 indicated the lowest and highest degree of polymerization of PCL block segment in these diblock copolymers, respectively) and phenolic/DDSQ hybrids

https://doi.org/10.1021/acs.macromol.2c01585
Macromolecules 2022, 55, 8918−8930

(abbreviation as PDDSQ in Scheme S1)[68] are summarized in Tables S1 and S2.

Self-Assembled PDDSQ/EC Blends and Mesoporous PDDSQ Hybrids. Various amounts of PDDSQ (featuring various DDSQ cage compositions) and EC diblock copolymers (with various volume fractions of their PCL blocks) were stirred in THF until complete dissolution. The solution was placed in an Al pan, and the solvent was then slowly evaporated for 2 days at 45 °C, with the structure formed based on evaporation-induced self-assembly. The resulting solid compound was heated at 150 °C for 1 day to provide the self-assembled structures of PDDSQ/EC hybrids through thermal curing polymerization (Scheme 1c). The EC diblock copolymers were subsequently removed through pyrolysis at 400 °C for 1 day to obtain the mesoporous PDDSQ hybrids (Scheme 1d).

RESULTS AND DISCUSSION

FTIR Spectra and SAXS Analyses of PDDSQ-25/EC Blends. In previous reports, we have widely discussed the hydrogen-bonding interactions of phenolic OH groups with ether units of PEO block and the C═O units of PCL block.[69−71] For convenience, in this study, we selected the PDDSQ-25/EC2, PDDSQ-25/EC3, and PDDSQ-25/EC4 blends as examples for FTIR spectral analyses, as displayed in Figure S4. The spectrum of pure PDDSQ-25 containing 25 mol % DDSQ displayed two signals for its OH groups at 3545 and 3385 cm^{-1}, representing free and self-association hydrogen-bonded OH units, respectively. The intensity of free OH units was decreased upon increasing the content of the EC copolymer; the signal for the self-associated OH units was shifted to lower wavenumber (to 3240 cm^{-1}), because of the OH···ether intermolecular hydrogen bonding, at lower PDDSQ contents, whereas it became broad at higher PDDSQ contents because of hydrogen bonding with both the PEO and PCL blocks. Because the intermolecular hydrogen bonding in PDDSQ/PEO blends (K_A = 264) is stronger than that in PDDSQ/PCL blends (K_A = 116), as we have discussed widely in previous reports,[59,69−71] the phenolic OH units were preferred to interact with PEO block at lower PDDSQ concentrations; however, they interacted with both PEO and PCL blocks at relative higher PDDSQ contents.

Most importantly, the C═O units of PCL block segments in EC diblock copolymers were sensitive to the presence of the phenolic OH groups in the PDDSQ hybrids (Figure 1). FTIR spectra of the pure EC diblock copolymers all featured two absorptions at 1734 and 1724 cm^{-1}, representing the amorphous (or free) and crystalline C═O units, respectively.[69,70] Upon increasing the PDDSQ-25 concentration to 50 wt %, the absorption for the crystalline C═O groups at 1724 cm^{-1} disappeared for the PDDSQ-25/EC2 and PDDSQ-25/EC3 blends (Figure 1a,b), but it remained for the PDDSQ-25/EC4 blend (Figure 1c), indicating that an increase in the molecular weight of PCL block in EC diblock copolymer led to the decrease in the fraction of C═O groups hydrogen bonding with phenolic OH groups as expected. Further increasing the PDDSQ-25 content to greater than 60 wt % led to another new absorption appearing near 1703 cm^{-1} due to the intermolecularly hydrogen-bonded C═O units of the PCL segment. The fraction of hydrogen-bonded C═O units could be determined through curve fitting, revealing that it increased upon increasing the PDDSQ compositions in these three PDDSQ-25/EC blends. Figure 1d summarizes the hydrogen-bonded C═O fractions in all of these PDDSQ-25/EC blends; these values increased upon increasing the PDDSQ content

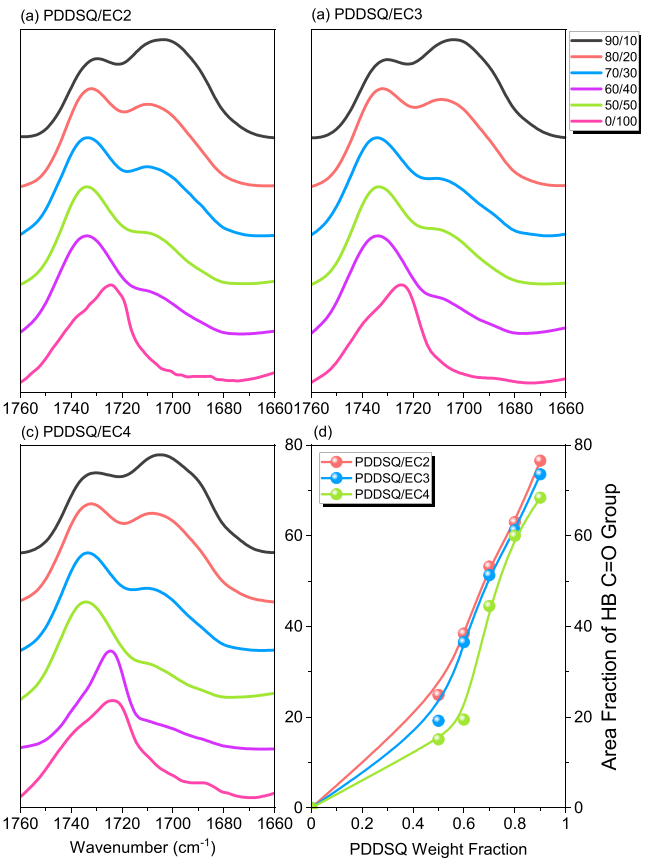

Figure 1. (a−c) FTIR spectra for C═O absorption recorded at room temperature of (a) PDDSQ/EC2, (b) PDDSQ/EC3, and (c) PDDSQ/EC4 blends after thermal curing at 150 °C. (d) Area fraction of the hydrogen-bonded C═O units in PDDSQ/EC-*x* blends.

but decreased upon increasing the molecular weight of the PCL block in the EC diblock copolymers, as expected.

To examine their self-assembled structures of PDDSQ-25/EC blends after thermal curing at 150 °C, Figure 2 and Figure S5 present their SAXS patterns. The pure EC diblock copolymers possessed LAM character, with SAXS peak ratios of 1:2, as displayed in Scheme 2a; this character was confirmed using TEM.[60−67] All of the PDDSQ-25/EC1 blends possessed micelle spherical structures based on their single broad peaks, as displayed in Figure S5. Because the low molecular weight (low N) of the PCL block would enhance the weak segregation strength (low χN), these blends displayed the short-range order of spherical structures. Figure 2 reveals the behavior of the other EC diblock copolymers as templates. At a PDDSQ-25 concentration of 50 wt %, the long-range order of the LAM structure was evident in Figure 2a−d, with peak ratios of 1:2:3 and the first-order q^* peaks shifted to slightly lower q values, indicating that the content of the micro-phase domain increased with the increase of molecular weight of PCL block in EC diblock copolymers as expected. Increasing the PDDSQ content to 60 wt % resulted in the long-range order of bicontinuous DG structures being observed, with the peak ratio of $\sqrt{2}:\sqrt{6}:\sqrt{8}:\sqrt{14}:\sqrt{16}:\sqrt{20}:\sqrt{22}:\sqrt{24}$ appearing in the pattern of the PDDSQ-25/EC2 = 60/40 blend in Figure 2e. The other PDDSQ-25/EC3, PDDSQ-25/EC4, and PDDSQ-25/EC5 = 60/40 blends all retained LAM structures, with peak ratios of 1:2:3 (Figure 2f,h). Further increasing the PDDSQ

https://doi.org/10.1021/acs.macromol.2c01585
Macromolecules 2022, 55, 8918−8930

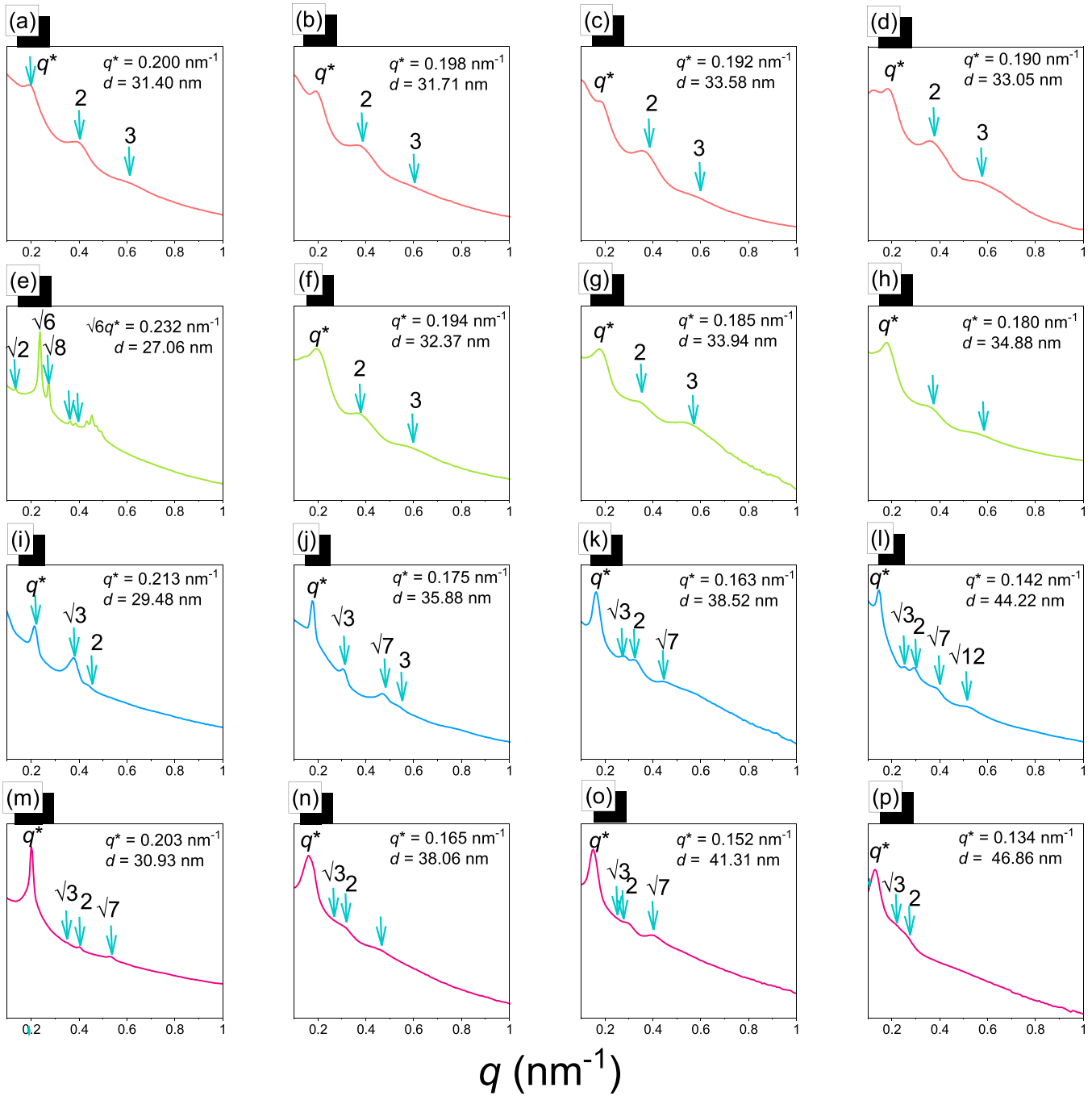

Figure 2. SAXS patterns of PDDSQ-25/EC blends after thermal curing at 150 °C: (a–d) 50/50, (e–h) 60/40, (i–l) 70/30, and (m–p) 80/20 blends with (a, e, i, m) EC2, (b, f, j, n) EC3, (c, g, k, o) EC4, and (d, h, l, p) EC5.

concentration to 70 and 80 wt % resulted in the appearance of peak ratios of $1:\sqrt{3}:\sqrt{4}$, and even $\sqrt{7}$, $\sqrt{9}$, or $\sqrt{12}$, being observed (Figure 2i–p), indicating that all of the blends possessed the long-range order of HEX structures. Furthermore, the patterns of all of the PDDSQ-25/EC = 90/10 blends also featured a single broad peak, similar to those in Figure S5, indicating the presence of micelle spherical structures (for brevity, data not shown). Based on the SAXS analyses in Figure 2, we conclude that the *d*-spacing increased upon increasing the molecular weight of the PCL block in the EC diblock copolymers. For example, the *d*-spacing increased from 30.63 to 39.74 nm upon proceeding from the PDDSQ/EC2 to PDDSQ/EC5 = 70/30 blend, because the hydrogen-bonded C═O fraction was decreased upon increasing the molecular weight of PCL block in EC diblock copolymer; thus, the domain size of the HEX structure formed from free isolated PCL domain would expand as displayed in Scheme 2b.

More interestingly, we observed the DG structure for the PDDSQ-25/EC2 = 60/40 blend system in Figure 2e. As mentioned above, only HEX and BCC self-assembled structures have formed when using the EC2 diblock copolymer as the template for silica and phenolic/silica hybrids, with the DG structure never observed; in contrast, the DG structure has been obtained in mesoporous phenolic resin. As a result, we became interested in examining the evolution of the DG structure for this present blend system. Figure 3 displays the in

https://doi.org/10.1021/acs.macromol.2c01585
Macromolecules 2022, 55, 8918–8930

Scheme 2. Possible Self-Assembled Structures, Hydrogen-Bonding Interactions, and Mesopore Sizes for PDDSQ/EC System Prepared with Various Molecular Weights of the PCL Block in the EC Diblock Copolymers

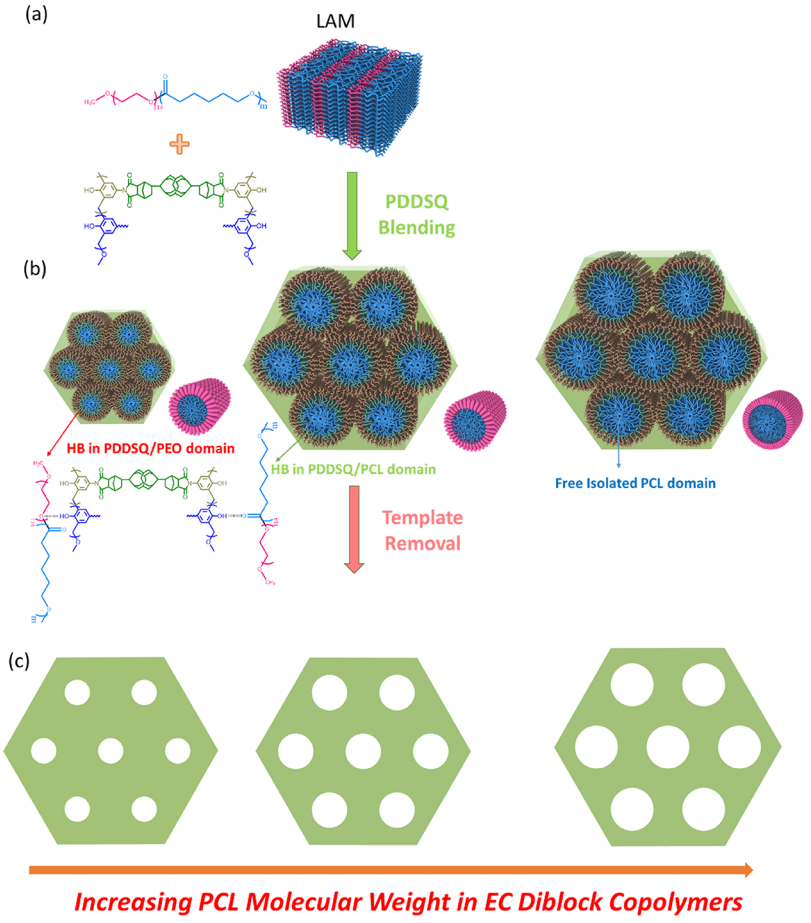

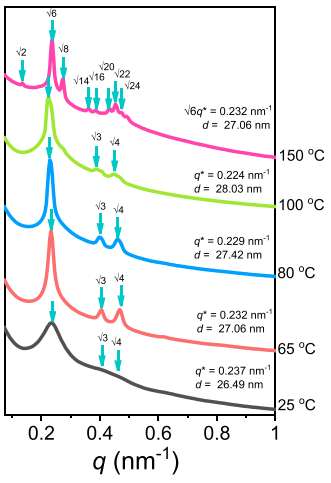

Figure 3. In situ SAXS patterns of PDDSQ/EC2 = 60/40 blends, recorded after thermal curing at various temperatures.

situ SAXS patterns determined during the thermal curing procedure. At room temperature, we observed the short-range order of the HEX structure, with peak ratios of $1:\sqrt{3}:\sqrt{4}$; increasing the temperature to 65 °C (above the melting points of the PEO and PCL blocks), we observed the long-range order of the HEX structure because the crystalline domain effect of the PEO and PCL segments had disappeared. The first peak shifted to a lower value of q (d = 26.49 nm at 25 °C) upon increasing the thermal curing temperature to 100 °C (d = 28.03 nm) because of the thermal expansion, as expected. After thermal curing at 150 °C, the long-range order of a bicontinuous DG structure was observed with peak ratios of $\sqrt{2}:\sqrt{6}:\sqrt{8}:\sqrt{14}:\sqrt{16}:\sqrt{20}:\sqrt{22}:\sqrt{24}$. This phenomenon is the result of so-called "reaction-induced microphase separation" in thermoset/thermoplastic blend systems.[72−75] During thermal curing, the molecular weight of PDDSQ would increase significantly and the entropy of mixing would decrease significantly, resulting in an unfavorable Gibbs free energy and, thus, microphase separation from the block copolymers. Because the DG structure is generally observed in the weak-segregation region (low χN), the lower molecular weight of the PCL block in the EC2 diblock copolymer (EC2) may have induced the presence of the DG structure in the PDDSQ matrix, a structure that we did not observe with EC3, EC4, and EC5. A high-molecular-weight EC diblock copolymer used as a template to form phenolic/silica hybrids could be considered to be providing a high value of χN because the inorganic silica or POSS cage would induce a high value of χ due to immiscibility with the organic polymer matrix.

Figure 4 summarizes the phase diagram of all the PDDSQ/EC blends featuring different molecular weights for the PCL block in the EC diblock copolymers. With the lowest molecular weight of PCL found in the EC1 diblock copolymer, most of its blend compositions featured the micelle spherical structure, with the only disorder structure appearing for PDDSQ-25/EC1 = 90/10. The PDDSQ-25/EC2 blend system

https://doi.org/10.1021/acs.macromol.2c01585
Macromolecules 2022, 55, 8918−8930

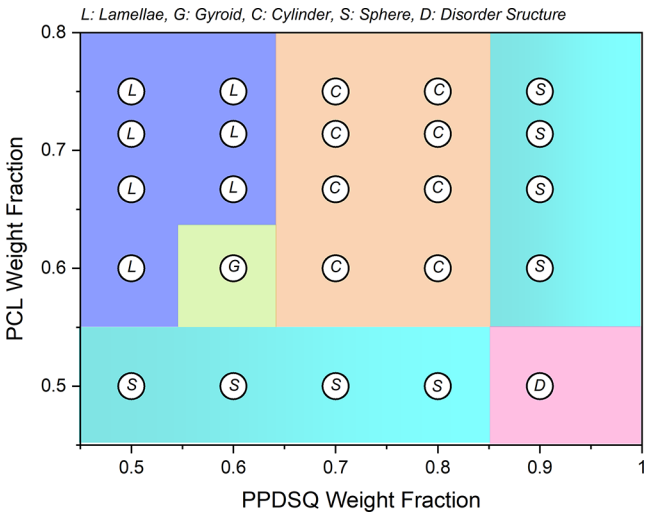

Figure 4. Phase diagram of the PDDSQ/EC blends after thermal curing at 150 °C based on data from SAXS patterns.

formed a full array of self-assembled structures, extending from LAM, DG, HEX, and finally to spherical structures. Increasing the molecular weight of the PCL block in the EC diblock copolymers to give EC3, EC4, and EC5 resulted in only the LAM, HEX, and spherical structures being observed, consistent with the predicted phase diagram.[69] As a result, we conclude that the PDDSQ/EC blend system displayed wet-brush behavior[76,77] because the self-assembled structures were readily tuned upon increasing PDDSQ content due to intermolecular hydrogen bonding of the phenolic OH groups of PDDSQ with both the PEO and PCL blocks, as displayed in Scheme 2b.

Mesoporous PDDSQ Hybrids. After thermal curing, we used thermal calcination to remove the EC templates and obtain mesoporous PDDSQ-25 hybrids. Figure 5 compares the SAXS patterns recorded before and after the calcination procedure. The first peaks shifted to higher values of q after thermal calcination of both PDDSQ-25/EC2 = 60/40 and PDDSQ-25/EC4 = 70/30, indicating that the domain size of

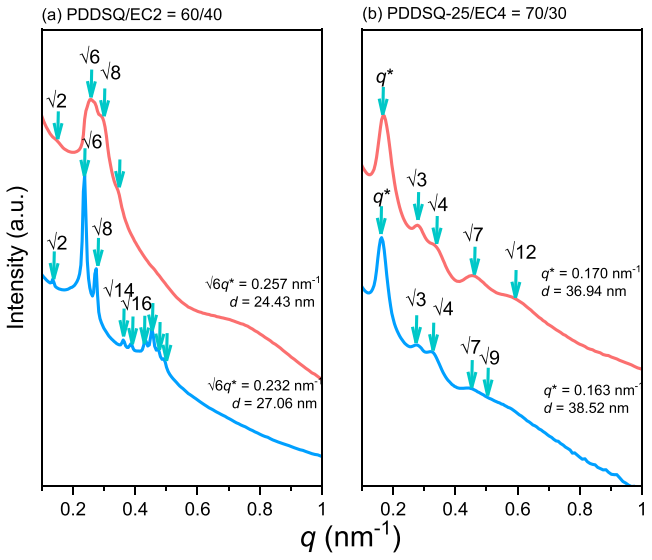

Figure 5. SAXS patterns of (a) PDDSQ-25/EC2 = 60/40 and (b) PDDSQ-25/EC3 = 80/20 recorded before and after thermal calcination at 400 °C.

the mesoporous materials had decreased due to shrinkage of the PDDSQ framework during the thermal calcination, as expected. Figure S6 presents the SAXS patterns of the mesoporous PDDSQ hybrids templated by the PDDSQ-25/EC-x = 50/50 and PDDSQ-25/EC-x = 90/10 blends. We obtained disordered patterns for the mesoporous PDDSQ hybrids templated at a 50 wt % PDDSQ content (Figure S6a), originally featuring LAM structures (Figure 2a–d); thus, the LAM structures were presumably destroyed, forming silt structures or disordered mesoporous structures.

Figure 6 presents the SAXS patterns and TEM images of the mesoporous PDDSQ hybrids templated by the various EC block copolymers at 60 wt % PDDSQ-25 content. For the mesoporous PDDSQ hybrid templated from PDDSQ-25/EC1 = 60/40, Figure 6a reveals the short-range order of micelle spherical structures based on the single broad peak, as confirmed through TEM analysis in Figure 6f. Figure 6k presents the N_2 adsorption/desorption isotherms of these mesoporous PDDSQ hybrids recorded at 77 K. The isotherms featured typical type IV curves, with values of P/P_0 ranging from 0.40 to 0.80 for the capillary condensation step and H_2 hysteresis loops observed in the relative pressure range from 0.4 to 0.7, implying inkbottle-shaped pore structures. Figure 6b,c displays the SAXS patterns of the mesoporous PDDSQ hybrids formed from PDDSQ/EC2 and PDDSQ/EC3 = 60/40, indicating the long-range order of DG structures with peak ratios of $\sqrt{wi}:\sqrt{6}:\sqrt{8}:\sqrt{14}$ and $\sqrt{6}:\sqrt{8}$, respectively, as confirmed from the TEM images in Figure 6g,h. Figure 6l,m provides the corresponding N_2 adsorption/desorption isotherms of these three mesoporous PDDSQ hybrids recorded at 77 K. The typical type IV curves featured sharp capillary condensation steps at values of P/P_0 from 0.85 to 0.95 and H_1 hysteresis loops in the relative pressure range from 0.4 to 0.9, implying the presence of large and branched cylindrical pore structures as well as the presence of mesoporous DG structures.

Further increasing the molecular weight of the PCL block in the templating EC diblock copolymer, Figure 6d,e displays the long-range order of mesoporous HEX structures with peak ratios of $1:\sqrt{3}:\sqrt{4}:\sqrt{7}:\sqrt{9}$, as confirmed in the TEM images in Figure 6i,j and the corresponding N_2 adsorption/desorption isotherms in Figure 6n,o. Again, the typical type IV curves revealed sharp capillary condensation steps at values of P/P_0 from 0.85 to 0.95, but in these cases, we observed H_{2a} hysteresis loops appearing in the relative pressure range from 0.4 to 0.9, suggesting the presence of large buckled cylindrical and cage-like mesoporous structures. The mesoporous PDDSQ hybrids prepared at 60 wt % PDDSQ content and templated by EC2 possessed the same DG structure as that prior to thermal calcination, as revealed in Figure 4. In contrast, we obtained mesoporous DG and HEX structures for the PDDSQ hybrids templated from the LAM structures of PDDSQ-25/EC3 and PDDSQ/EC4 = 60/40, respectively. This result is similar to that reported previously for the mesoporous phenolic resin templated from the PEO-*b*-PCL-*b*-PLLA triblock copolymer at a 30 wt % content of phenolic resin, where an LAM to DG or HEX structural transformation also occurred after thermal calcination.[78] This phenomenon can be explained by considering that the domain sizes of PDDSQ/EC = 60/40 blends likely decreased during thermal calcination and that the fraction of hydrogen-bonded C═O groups in the PCL segment decreased upon increasing the

https://doi.org/10.1021/acs.macromol.2c01585
Macromolecules 2022, 55, 8918–8930

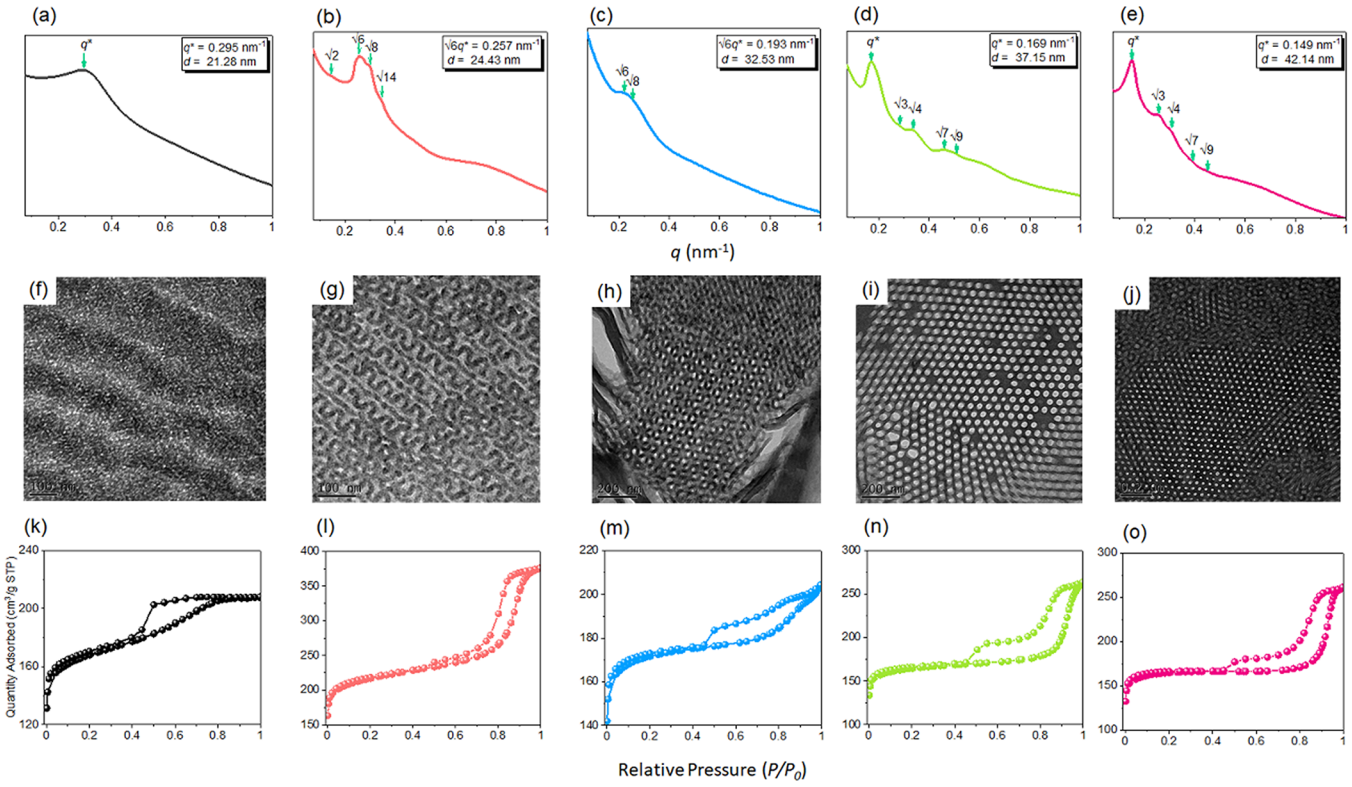

Figure 6. (a–e) SAXS patterns and (f–j) TEM images recorded at room temperature and (k–o) N_2 sorption/desorption isotherms recorded at 77 K for mesoporous PDDSQ hybrids templated from PDDSQ/EC-x = 60/40 systems with (a, f, k) EC1, (b, g, l) EC2, (c, h, m) EC3, (d, i, n) EC4, and (e, j, o) EC5.

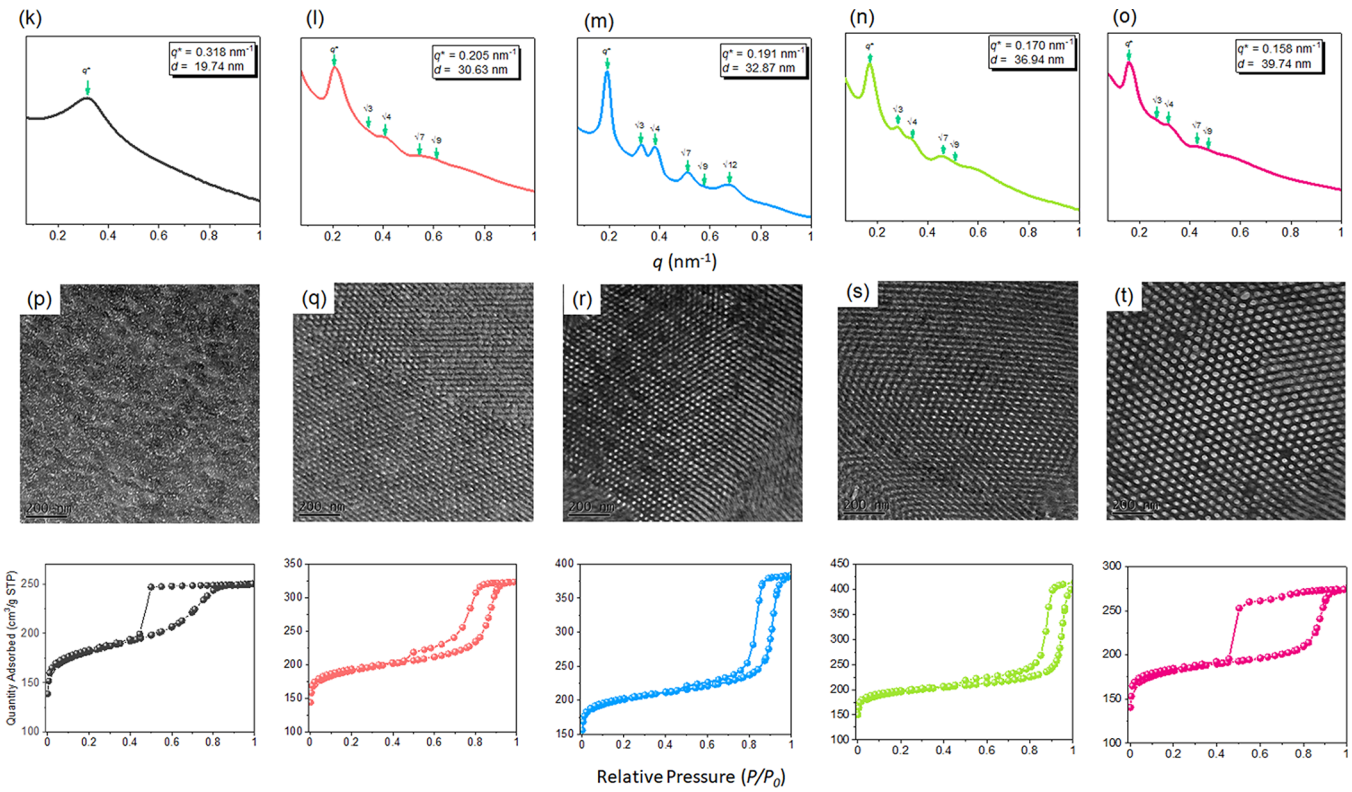

Figure 7. (a–e) SAXS patterns and (f–j) TEM images recorded at room temperature and (k–o) N_2 sorption/desorption isotherms recorded at 77 K for mesoporous PDDSQ hybrids templated from PDDSQ/EC-x = 70/30 systems with (a, f, k) EC1, (b, g, l) EC2, (c, h, m) EC3, (d, i, n) EC4, and (e, j, o) EC5.

https://doi.org/10.1021/acs.macromol.2c01585
Macromolecules 2022, 55, 8918–8930

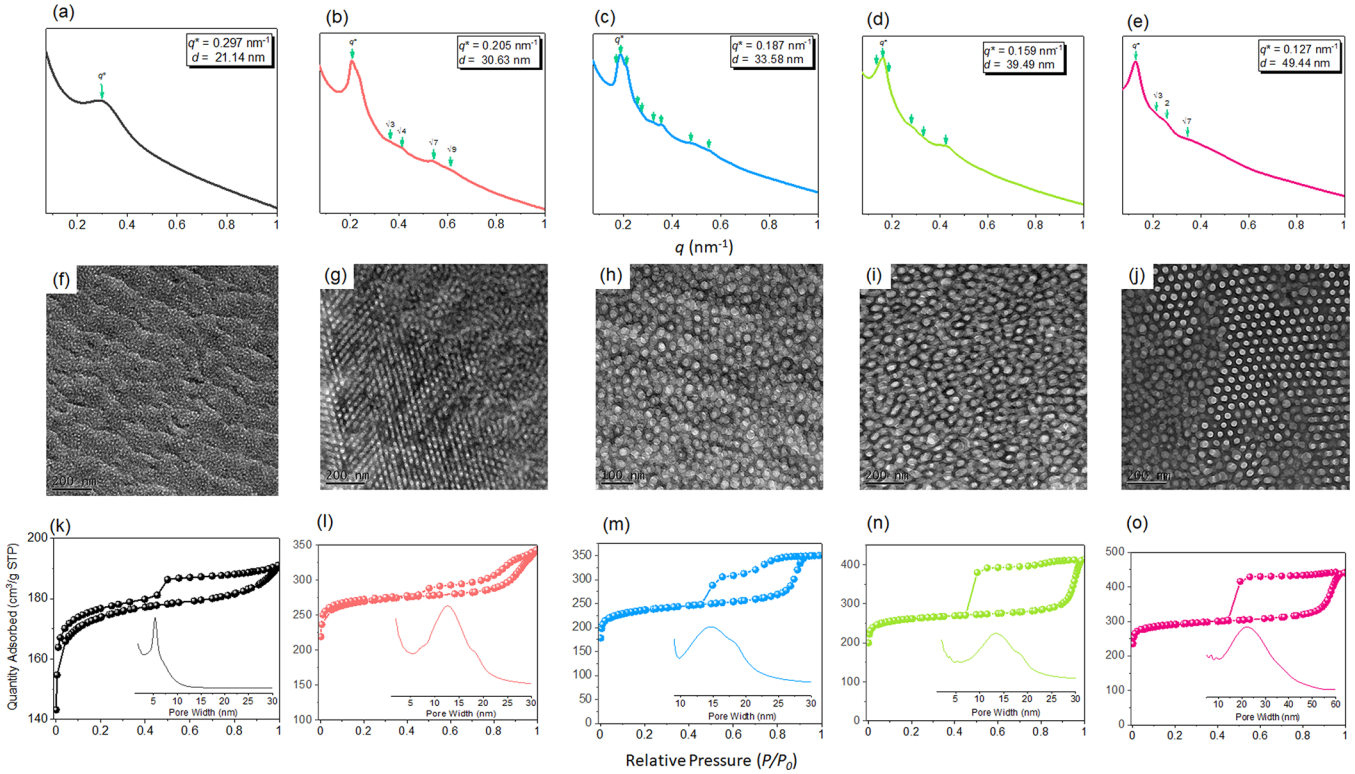

Figure 8. (a–e) SAXS patterns and (f–j) TEM images recorded at room temperature and (k–o) N_2 sorption/desorption isotherms recorded at 77 K for mesoporous PDDSQ hybrids templated from PDDSQ/EC-x = 80/20 systems with (a, f, k) EC1, (b, g, l) EC2, (c, h, m) EC3, (d, i, n) EC4, and (e, j, o) EC5.

molecular weight of the PCL block in EC diblock copolymer. To maintain the thermodynamically stable mesoporous structure, the shrinkage of the PDDSQ framework could then lead to the transformation to a DG or HEX structure due to minimization of the surface free energy and surface area upon proceeding from the LAM to DG or HEX structure. Nevertheless, this phenomenon did not occur for the LAM structures formed at 50 wt % PDDSQ content in the PDDSQ-25/EC blends, which all transformed into disordered mesoporous PDDSQ hybrids. At relatively lower PDDSQ contents (<50 wt %), the blend systems did not contain enough PDDSQ relative to the EC diblock copolymer; in addition, the fraction of hydrogen-bonded C═O groups of the PCL block was lower than that at higher PDDSQ contents, as displayed in Figure 1, and therefore, a disordered structure was formed.

Figure 7 presents the SAXS, TEM, and Brunauer–Emmett–Teller (BET) data of the mesoporous PDDSQ hybrids templated by various EC templates after increasing the PDDSQ content to 70 wt %.

Similar to the system in Figure 6a,f,k, the mesoporous PDDSQ hybrid templated from PDDSQ-25/EC1 = 70/30 also displayed the short-range order of a micelle spherical structure with inkbottle-shaped pore structures (Figure 7a,f,k). The SAXS patterns of the mesoporous PDDSQ hybrids prepared with other templates revealed the long-range order of HEX structures, with peak ratios of $1:\sqrt{3}:\sqrt{4}:\sqrt{7}:\sqrt{9}$ (Figure 7b–e), as confirmed by the TEM images in Figure 7g–j. Figure 7l–o presents the corresponding N_2 adsorption/desorption isotherms of these mesoporous PDDSQ hybrids recorded at 77 K. Each provided a typical type IV curve with an H_1 hysteresis loop, suggesting a large and branched cylindrical pore structure, namely, a mesoporous HEX structure; accordingly, these structures were the same (HEX) before and after thermal calcination, as displayed in Figure 4.

Figure 8 provides the SAXS, TEM, and BET data of the mesoporous PDDSQ hybrids templated by various EC block copolymers after further increasing the PDDSQ content to 80 wt %.

The SAXS pattern of the mesoporous PDDSQ hybrid templated from EC1 (Figure 8a) featured a single broad peak, suggesting a spherical micelle structure as confirmed by the TEM image in Figure 8f. Its corresponding N_2 adsorption/desorption isotherm (Figure 8k) revealed a typical type IV curve with the H_{2a} hysteresis loop, indicating a cage-like mesoporous structure. Figure 8b displays the SAXS pattern of the mesoporous PDDSQ hybrid templated from EC2, revealing an HEX structure with a peak ratio of $1:\sqrt{3}:\sqrt{4}:\sqrt{7}:\sqrt{9}$; this structure was confirmed by the TEM image in Figure 8g. The corresponding N_2 adsorption/desorption isotherm in Figure 8l reveals a typical type IV curve with an H_1 hysteresis loop, indicating a cylindrical-like mesoporous structure. Figure 8c,d displays multiple peak ratios, indicating the presence of local FK σ and Z phases as confirmed by the TEM images in Figure 8h,i. The detailed scheme of the TEM image along the [001] direction of the FK σ phase, featuring a typical $3^2.4.3.4$ tiling number, is provided in Figure S7a; that of the FK Z phase, featuring a typical 3^6 tiling number, is presented in Figure S7b. Their corresponding N_2 adsorption/desorption isotherms (Figure 8m,n) also revealed typical IV curves with H_1-like hysteresis loops; nevertheless, two sharp hysteresis curves could be observed during the desorption procedure in the relative pressure ranges from 0.80 to 0.70 and from 0.70 to 0.40, suggesting two kinds of ordered mesopore

https://doi.org/10.1021/acs.macromol.2c01585
Macromolecules 2022, 55, 8918–8930

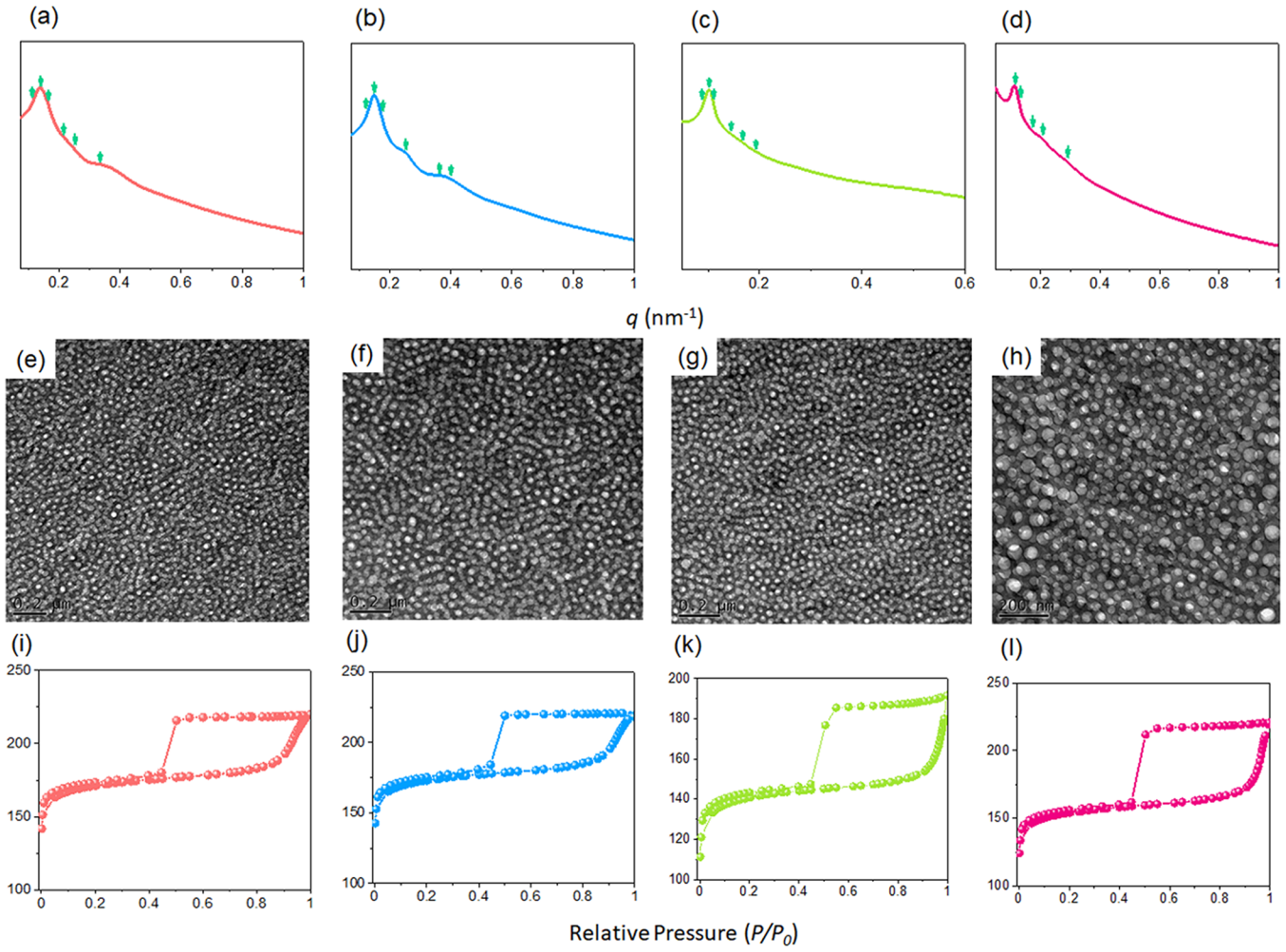

Figure 9. (a–d) SAXS patterns and (e–h) TEM images measured at room temperature and (i–l) N_2 sorption/desorption isotherms recorded at 77 K for mesoporous PDDSQ hybrids templated from PDDSQ-*x*/EC5 = 90/10 systems with (a, e, j) PDDSQ-1, (b, f, j) PDDSQ-2, (c, g, k) PDDSQ-3, and (d, h, l) PDDSQ-4.

sizes as displayed in the insets of Figure 8m,n.[79] The mean pore sizes based on the Harkins and Jura model were 14.8 and 18.2 nm in Figure 8m and 13.3 and 18.1 nm in Figure 8n, with the smaller and larger pore sizes corresponding to CNs of 12 and 14 spheres, respectively. Upon increasing the molecular weight of the PCL block in the EC diblock copolymer, the pore size arising from the CN of 14 spheres increased as expected. This result is consistent with our PDDSQ-30/EC3 system, which also displayed the FK phases.[59] Further increasing the molecular weight of the PCL in the EC5 diblock copolymer caused the system to return to a highly ordered HEX structure, with a peak ratio of $1:\sqrt{3}:\sqrt{4}:\sqrt{7}$ in the SAXS pattern (Figure 8e) as confirmed by the TEM image in Figure 8j; its N_2 adsorption/desorption isotherm also featured a typical type IV curve with an H_1 hysteresis loop, indicating that a cylindrical-like mesoporous structure had again formed. Most importantly, the PDDSQ hybrids formed at an 80 wt % PDDSQ content and templated by EC2 and EC5 displayed the same HEX structure both before and after thermal calcination, as displayed in Figure 4; in contrast, they transformed to the mesoporous FK σ phase from the HEX structure when templated by EC3 and EC4. Again, we suggest the same explanation as that for the systems prepared with PDDSQ at 60 wt %: that shrinkage of the PDDSQ framework led to the transformation to the FK spherical structure due to minimization of the surface free energy and surface area upon proceeding from the HEX structure to the FK spherical structure. Nonetheless, the system returned to the HEX structure when templated by the EC5 diblock copolymer; here, because the copolymer featured the highest molecular weight of the PCL block and the lowest fraction of hydrogen-bonded C═O groups in its PCL block, the volume fraction of the isolated PCL domain was too large and thus could not form the FK spherical structure.

Furthermore, the transformation from a disordered structure to a long-range-ordered spherical structure occurred upon increasing the molecular weight of the PCL block in the templating EC diblock copolymer when preparing mesoporous PDDSQ hybrids templated at a 90 wt % PDDSQ content (Figure S8b). In addition, the *d*-spacing of these mesoporous hybrids increased, and more ordered mesoporous structures formed with multiple scattering peaks when the molecular weight of the PCL block in the EC diblock copolymer increased in the PDDSQ/EC-*x* = 90/10 blends (Figure S8b). For example, the mesoporous PDDSQ hybrid templated from PDDSQ-25/EC5 = 90/10 provided a peak ratio of $1:\sqrt{3}:\sqrt{7}$ and a *d*-spacing of 47.57 nm, much higher than that for PDDSQ-25/EC2 = 90/10 (42.72 nm) with a single broad

https://doi.org/10.1021/acs.macromol.2c01585
Macromolecules 2022, 55, 8918−8930

peak. Accordingly, we inferred that the volume fraction of the isolated PCL domain should further decrease for the various mesoporous PDDSQ hybrids prepared from the PDDSQ-*x*/EC5 = 90/10 blends. Here, all of the SAXS patterns and TEM images (Figure 9a–h) revealed local FK phases regardless of the DDSQ content in the PDDSQ hybrids; in addition, the N_2 adsorption/desorption isotherms revealed typical type IV curves with H_1 hysteresis loops, indicating cage-like mesoporous structures as displayed in Figure 9i–l.

Table 1 and Table S3 summarize the SAXS and BET data of all of the mesoporous PDDSQ hybrids prepared in this study.

Table 1. The Properties of Mesoporous PDDSQ Hybrids Templated by EC Diblock Copolymers in This Study Based on SAXS and N_2 Adsorption/Desorption Isotherm Analyses

samples	*d*-spacing (nm)	S_{BET} (m^2/g)	S_M (m^2/g)	pore volume (cm^3/g)	pore size (nm)
PDDSQ/EC1 = 6/4	21.28	524	388	0.32	5.2
PDDSQ/EC2 = 6/4	24.43	676	495	0.52	8.6
PDDSQ/EC3 = 6/4	32.53	525	448	0.31	12.6
PDDSQ/EC4 = 6/4	37.15	565	426	0.42	15.4
PDDSQ/EC5 = 6/4	42.14	509	426	0.40	20.8
PDDSQ/EC1 = 7/3	19.74	567	408	0.38	5.9
PDDSQ/EC2 = 7/3	30.63	601	429	0.49	12.6
PDDSQ/EC3 = 7/3	32.87	632	466	0.28	15.4
PDDSQ/EC4 = 7/3	36.94	609	450	0.61	18.8
PDDSQ/EC5 = 7/3	39.74	504	436	0.40	21.7
PDDSQ/EC1 = 8/2	21.14	719	602	0.39	6.2
PDDSQ/EC2 = 8/2	30.63	832	701	0.53	11.2
PDDSQ/EC3 = 8/2	33.58	732	560	0.59	14.8, 18.2
PDDSQ/EC4 = 8/2	39.49	805	651	0.63	13.3, 18.1
PDDSQ/EC5 = 8/2	49.44	902	740	0.68	23.2
PDDSQ/EC1 = 9/1		504	518	0.27	
PDDSQ/EC2 = 9/1	42.72	535	442	0.32	11.3
PDDSQ/EC3 = 9/1	46.17	501	432	0.32	14.6
PDDSQ/EC4 = 9/1	46.51	532	457	0.35	17.6
PDDSQ/EC5 = 9/1	47.57	489	410	0.30	8.6, 20.4

We make several conclusions. First, the *d*-spacings and pore sizes of these mesoporous PDDSQ hybrids increased upon increasing the molecular weight of the PCL block in the EC diblock copolymer templates. Second, all of the mesoporous PDDSQ hybrids in this study had high BET surface areas, mesoporous surface area (S_M), and pore volumes much higher than those of the mesoporous phenolic resins templated by similar PEO-*b*-PCL diblock copolymers in a previous study.[62] For example, the mesoporous PDDSQ hybrids templated from the PDDSQ/EC-*x* = 60/40 systems had surface areas ranging from 524 to 676 m^2/g, much higher than those of the mesoporous phenolic resins templated from phenolic/EC-*x* = 60/40 systems (only ranging from 61 to 137 m^2/g).[62]

This phenomenon can be explained by considering that the cage structure of DDSQ may have provided the additional pore volume and surface area to the porous structure. Third, the surface areas and pore volumes of the mesoporous PDDSQ hybrids templated from the PDDSQ/EC-*x* = 80/20 systems were generally higher than those of their blend compositions, indicating that the closed packing of the spherical porous structures of the FK phases provided higher BET surface areas, mesoporous surface areas, and pore volumes when compared with those of the DG, HEX, and only BCC spherical structures. In addition, the HEX and FK mesoporous structures also have higher surface area compared with other mesoporous structures. Finally, the existence of the mesoporous FK phase in this system was strongly dependent on the volume fraction of the isolated PCL domain, itself related to the molecular weight and fraction of hydrogen-bonded C=O groups of the PCL block.

Figure 10 summarizes the phase diagram of all of the mesoporous PDDSQ hybrids templated from all of the

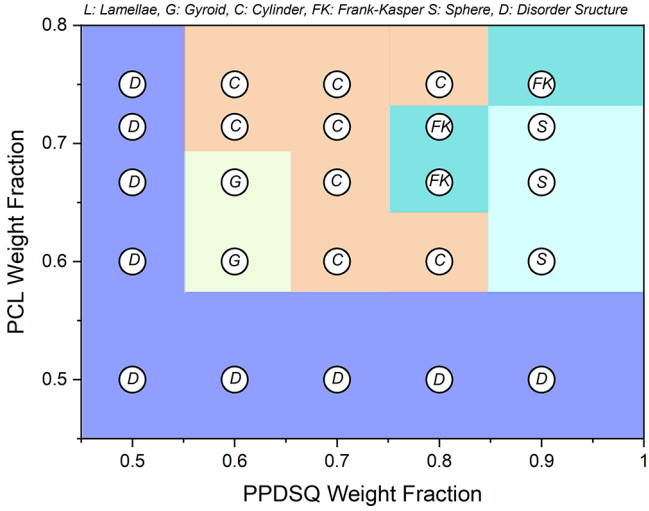

Figure 10. Phase diagram of mesoporous PDDSQ hybrids templated from PDDSQ/EC blends after thermal calcination at 400 °C based on data from SAXS patterns and TEM images.

PDDSQ-25/EC blends with various molecular weights for the PCL block in the EC diblock copolymers. Again, we reach several conclusions. First, the phase diagram of the mesoporous PDDSQ hybrids was different from that of the PDDSQ/EC blends (Figure 4), suggesting a different type of self-assembly during thermal calcination. Shrinkage of the PDDSQ framework could lead to transformations from LAM structures to DG or HEX structures and from HEX to FK spherical structures due to minimization of the surface free energy and surface area at certain PDDSQ/EC blend compositions as displayed in Scheme 1d. Second, a full phase transition could be obtained in the mesoporous PDDSQ hybrids, from a disordered structure to DG, HEX, FK, and spherical structures especially in the PDDSQ/EC3 blend system. Third, the phase behavior was strongly dependent on the PDDSQ content and the molecular weight of the PCL block in the EC diblock copolymer; it was correlated to the volume fraction of the isolated PCL domains, itself influenced by the fraction of hydrogen-bonded and free C=O groups in the PCL block as displayed in Scheme 1c,d. For example, a lower molecular weight for the PCL block in the EC diblock copolymer could result in the formation of the DG structure but not at a higher molecular weight because this structure has generally been observed only in the weak-segregation region (low χN), whereas the FK phase existed only for higher molecular weights of the PCL block in the strong-segregation region (high χN) and for highly asymmetric block copolymer compositions. Finally, this study provides a general principle for the synthesis of tunable mesoporous structures by taking

https://doi.org/10.1021/acs.macromol.2c01585
Macromolecules 2022, 55, 8918–8930

into account completive hydrogen-bonding interactions and microphase separation behavior. A future study should reveal the detailed phase diagram of these PDDSQ-*x* systems upon changing the DDSQ cage content at various PEO-*b*-PCL molecular weights and other POSS composite with FK phases.[79−82]

CONCLUSIONS

We have synthesized a series of linear PEO-*b*-PCL diblock copolymers featuring various PCL molecular weights through ring-opening living polymerizations and prepared various PDDSQ hybrids. Competitive hydrogen-bonding interactions occurred between the OH groups of PDDSQ and both the PEO and PCL blocks, with the fraction of hydrogen-bonded C═O groups of the PCL block increasing upon increasing the content of PDDSQ or decreasing the molecular weight of the PCL block in the EC diblock copolymer. SAXS analyses allowed us to obtain the detailed phase diagram of the PDDSQ/EC blends after thermal polymerization at 150 °C, with a full phase transformation from LAM to DG, HEX, and spherical structures occurring because of wet-brush behavior upon changing the volume fraction of the isolated PCL domains as a result of the competitive hydrogen-bonding interaction. After removing the templating EC diblock copolymers, we obtained mesoporous phenolic/DDSQ hybrids having high surface areas and pore volumes, with a range of highly ordered mesoporous structures, including DG, HEX, spherical, and even FK structures, as influenced by the molecular weight of the PCL block and the content of PPDSQ hybrids. Overall, this study provides a general principle for obtaining mesoporous DG and FK phases mediated by the composition of a block copolymer, thereby influencing competitive hydrogen-bonding interactions.

ASSOCIATED CONTENT

Supporting Information

The Supporting Information is available free of charge at https://pubs.acs.org/doi/10.1021/acs.macromol.2c01585.

Characterization methods, ^{1}H and ^{13}C NMR spectra of PEO-*b*-PCL diblock copolymers and FTIR spectra of PDDSQ hybrids. FTIR spectra of PDDSQ/EC blends after thermal curing. SAXS patterns of PDDSQ/EC1 blends, mesoporous PDDSQ hybrids from PDDSQ/EC-*x* = 50/50 and 90/10 blends and TEM images of mesoporous PDDSQ hybrids templated from PDDSQ/EC3 and PDDSQ/EC4 = 80/20 blends (PDF)

AUTHOR INFORMATION

Corresponding Author

Shiao-Wei Kuo − *Department of Materials and Optoelectronic Science, Center for Functional Polymers and Supramolecular Materials, National Sun Yat-Sen University, Kaohsiung 804, Taiwan;* orcid.org/0000-0002-4306-7171; Email: kuosw@faculty.nsysu.edu.tw

Authors

Yen-Chi Huang − *Department of Materials and Optoelectronic Science, Center for Functional Polymers and Supramolecular Materials, National Sun Yat-Sen University, Kaohsiung 804, Taiwan*

Wei-Cheng Chen − *Department of Materials and Optoelectronic Science, Center for Functional Polymers and Supramolecular Materials, National Sun Yat-Sen University, Kaohsiung 804, Taiwan*

Complete contact information is available at: https://pubs.acs.org/10.1021/acs.macromol.2c01585

Notes

The authors declare no competing financial interest.

ACKNOWLEDGMENTS

This study was supported financially by the Ministry of Science and Technology, Taiwan, under contracts MOST 111-2223-E-110-004 and 108-2221-E-110-014-MY3.

REFERENCES

(1) Mai, Y.; Eisenberg, A. Self-Assembly of Bock Copolymers. *Chem. Soc. Rev.* **2012**, *41*, 5969−5985.

(2) Klok, H. A.; Lecommandoux, S. Supramolecular materials via block copolymer self-assembly. *Adv. Mater.* **2001**, *13*, 1217−1229.

(3) Kim, J. K.; Yang, S. Y.; Lee, Y.; Kim, Y. Functional nanomaterials based on block copolymer self-assembly. *Prog. Polym. Sci.* **2010**, *35*, 1325−1349.

(4) Shin, J. J.; Kim, E. J.; Ku, K. H.; Lee, Y. J.; Hawker, C. J.; Kim, B. J. 100th Anniversary of Macromolecular Science Viewpoint: Block Copolymer Particles: Tuning Shape, Interfaces, and Morphology. *ACS Macro Lett.* **2020**, *9*, 306−317.

(5) Lin, E.-L.; Hsu, W.-L.; Chiang, Y.-W. Trapping Structural Coloration by a Bioinspired Gyroid Microstructure in Solid State. *ACS Nano* **2018**, *12*, 485−493.

(6) Su, H. W.; Lin, I. M.; Yeh, Y. J.; Chiang, Y. W. Detection of extremely low- and high-concentration organic acids by a highly-aligned lamellar block copolymer photonic crystal film. *Mater. Chem. Phys.* **2022**, *287*, No. 126256.

(7) Jo, S.; Jun, T.; Jeon, H. I.; Seo, S.; Kim, H.; Lee, S.; Ryu, D. Y. Optical Reflection from Unforbidden Diffraction of Block Copolymer Templated Gyroid Films. *ACS Macro Lett.* **2021**, *10*, 1609−1615.

(8) Goi, E.; Cumming, B. P.; Gu, M. Gyroid "srs" Networks: Photonic Materials Beyond Nature. *Adv. Opt. Mater.* **2018**, *6*, 181800485.

(9) Jin, X.; Zhang, C.; Lin, J.; Cai, C.; Chen, J.; Gao, L. Fusion Growth of Two-Dimensional Disklike Micelles via Liquid-Crystallization-Driven Self-Assembly. *Macromolecules* **2022**, *55*, 3831−3839.

(10) Tang, Z.; Gao, L.; Lin, J.; Cai, C.; Yao, Y.; Guerin, G.; Tian, X.; Lin, S. Anchorage-Dependent Living Supramolecular Self-Assembly of Polymeric Micelles. *J. Am. Chem. Soc.* **2021**, *143*, 14684−14693.

(11) Kuo, S. W. Hydrogen bonding mediated self-assembled structures from block copolymer mixtures to mesoporous materials. *Polym. Int.* **2022**, *71*, 393−410.

(12) Mohamed, M. G.; Kuo, S. W. Progress in the self-assembly of organic/inorganic polyhedral oligomeric silsesquioxane (POSS) hybrids. *Soft Matter* **2022**, *18*, 5535−5561.

(13) Tsou, C. T.; Kuo, S. W. Competing Hydrogen Bonding Interaction Creates Hierarchically Ordered Self-Assembled Structures of PMMA-*b*-P4VP/PVPh-*b*-PS Mixtures. *Macromolecules* **2019**, *52*, 8374−8383.

(14) Yu, Y.-G.; Seo, C.; Chae, C.-G.; Seo, H.-B.; Kim, M.-J.; Kang, Y.; Lee, J.-S. Hydrogen Bonding-Mediated Phase Transition of Polystyrene and Polyhydroxystyrene Bottlebrush Block Copolymers with Polyethylene Glycol. *Macromolecules* **2019**, *52*, 4349−4358.

(15) Kennemur, J. G. Poly(Vinylpyridine) Segments in Block Copolymers: Synthesis, Self-Assembly, and Versatility. *Macromolecules* **2019**, *52*, 1354−1370.

(16) Varlas, S.; Hua, Z.; Jones, J. R.; Thomas, M.; Foster, J. C.; O'Reilly, R. K. Complementary nucleobase interactions drive the hierarchical self-assembly of core−shell bottlebrush bock copolymers toward cylindrical supramolecules. *Macromolecules* **2020**, *53*, 9747−9757.

(17) Pan, H.; Zhang, W.; Xiao, A.; Lyu, X.; Shen, Z.; Fan, X. Persistent Formation of Self-Assembled Cylindrical Structure in a Liquid Crystalline Block Copolymer Constructed by Hydrogen Bonding. *Macromolecules* **2018**, *51*, 5676−5684.
(18) Wong, C. K.; Qiang, X.; Müller, A. H. E.; Gröschel, A. H. Self-Assembly of block copolymers into internally ordered microparticles. *Prog. Polym. Sci.* **2020**, *102*, No. 101211.
(19) Sikder, A.; Ghosh, S. Hydrogen-bonding regulated assembly of molecular and macromolecular amphiphiles. *Mater. Chem. Front.* **2019**, *3*, 2602−2616.
(20) Shin, N.; Ahn, S.; Kim, E.; Kim, E. Y.; Park, S. Y.; Lee, J.; Kim, J. K. Nucleobase-Containing Block Copolymers Having a High Interaction Parameter by Complementary Hydrogen Bonding. *Macromolecules* **2021**, *54*, 4564−4570.
(21) Li, X.; Xu, W.; Chang, X.; Zheng, Y.; Ni, L.; Shan, G.; Bao, Y.; Pan, P. Stepwise Crystallization and Induced Microphase Separation in Nucleobase-Monofunctionalized Supramolecular Poly(ε-caprolactone). *Macromolecules* **2021**, *54*, 846−857.
(22) Han, S. H.; Kim, J. K.; Pryamitsyn, V.; Ganesan, V. Phase Behavior of Binary Blends of Block Copolymers Having Hydrogen Bonding. *Macromolecules* **2011**, *44*, 4970−4976.
(23) EL-Mahdy, A. F. M.; Yu, T. C.; Kuo, S.-W. Synthesis of Multiple Heteroatom−Doped Mesoporous Carbon/Silica Composites for Supercapacitors. *Chem. Eng. J.* **2021**, *414*, No. 128796.
(24) EL-Mahdy, A. F. M.; Yu, T. C.; Mohamed, M. G.; Kuo, S.-W. Secondary Structures of Polypeptide-Based Diblock Copolymers Influence the Microphase Separation of Templates for the Fabrication of Microporous Carbons. *Macromolecules* **2021**, *54*, 1030−1042.
(25) Chen, W.-C.; Tsao, Y.-H.; Wang, C.-F.; Huang, C.-F.; Dai, L.; Chen, T.; Kuo, S.-W. Main Chain−Type Block Copolymers through Atom Transfer Radical Polymerization from Double-Decker−Shaped Polyhedral Oligomeric Silsesquioxane Hybrids. *Polymer* **2020**, *12*, 465.
(26) Lee, S.; Bluemle, M. J.; Bates, F. S. Discovery of a Frank-Kasper σ Phase in Sphere-Forming Block Copolymer Melts. *Science* **2010**, *330*, 349−353.
(27) Takagi, H.; Yamamoto, K. Phase Boundary of Frank-Kasper σ Phase in Phase Diagrams of Binary Mixtures of Block Copolymers and Homopolymers. *Macromolecules* **2019**, *52*, 2007−2014.
(28) Dorfman, K. D. Frank-Kasper Phases in Block Polymers. *Macromolecules* **2021**, *54*, 10251−10270.
(29) Ma, Z.; Tan, R.; Gan, Z.; Zhou, D.; Yang, Y.; Zhang, W.; Dong, X.-H. Modulation of the Complex Spherical Packings through Rationally Doping a Discrete Homopolymer into a Discrete Block Copolymer: A Quantitative Study. *Macromolecules* **2022**, *55*, 4331−4340.
(30) Reddy, A.; Buckley, M. B.; Arora, A.; Bates, F. S.; Dorfman, K. D.; Grason, G. M. Stable Frank-Kasper Phases of Self-Assembled, Soft Matter Spheres. *Proc. Natl. Acad. Sci. U. S. A.* **2018**, *115*, 10233−10238.
(31) Watanabe, M.; Asai, Y.; Suzuki, J.; Takano, A.; Matsushita, Y. Frank-Kasper A15 Phase Formed in AB_n block-graft copolymers with large numbers of graft chains. *Macromolecules* **2020**, *53*, 10217−10224.
(32) Zhao, M.; Li, W. Laves Phases Formed in the Binary Blend of AB_4 Miktoarm Star Copolymer and A-Homopolymer. *Macromolecules* **2019**, *52*, 1832−1842.
(33) Xie, J.; Shi, A.-C. Formation of complex spherical packing phases in diblock copolymer/homopolymer blends. *Giant* **2021**, *5*, No. 100043.
(34) Zhao, B.; Wang, C.; Chen, Y.; Liu, M. Frank-Kasper phases self-assembled from linear $A_1B_1A_2B_2$ tetrablock copolymer. *Langmuir* **2021**, *37*, 5642−5650.
(35) Huang, M.; Yue, K.; Wang, J.; Hsu, C. H.; Wang, L.; Cheng, S. Z. D. Frank-Kasper and related quasicrystal spherical phases in macromolecules. *Sci. China: Chem.* **2018**, *61*, 33−45.
(36) Liu, Y.; Liu, T.; Yan, X.-y.; Guo, Q.-Y.; Wang, J.; Zhang, R.; Zhang, S.; Su, Z.; Huang, J.; Liu, G.-x.; Zhang, W.; Zhang, W.; Aida, T.; Yue, K.; Huang, M.; Cheng, S. Z. D. Mesoatom Alloys via Self-sorting Approach of Giant, Molecules Blends. *Giant* **2020**, *4*, No. 100031.
(37) Lee, S.; Leighton, C.; Bates, F. S. Sphericity and symmetry breaking in the formation of Frank-Kasper phases from one component materials. *Proc. Natl. Acad. Sci. U. S. A.* **2014**, *111*, 17723−17731.
(38) Su, Z.; Huang, M.; Cheng, S. Z. D. Complex self-assembled lattices from simple polymer blends. *Proc. Natl. Acad. Sci. U. S. A.* **2020**, *117*, 19618−19620.
(39) Xie, S.; Lindsay, A. P.; Bates, F. S.; Lodge, T. P. Formation of a C15 Laves Phase with a Giant Unit Cell in Salt-Doped A/B/AB Ternary Polymer Blends. *ACS Nano* **2020**, *14*, 13754−13764.
(40) Gillard, T. M.; Lee, S.; Bates, F. S. Dodecagonal quasicrystalline order in a diblock copolymer melt. *Proc. Natl. Acad. Sci. U. S. A.* **2016**, *113*, 5167−5172.
(41) Jeon, S.; Jun, T.; Jo, S.; Ahn, H.; Lee, S.; Lee, B.; Ryu, D. Y. Frank-Kasper Phases Identified in PDMS-b-PTFEA Copolymers with High Conformational Asymmetry. *Macromol. Rapid Commun.* **2019**, *40*, 1900259.
(42) Kim, K.; Schulze, M. W.; Arora, A.; Lewis, R. M., III; Hillmyer, M. A.; Dorfman, K. D.; Bates, F. S. Thermal processing of diblock copolymer melts mimics metallurgy. *Science* **2017**, *356*, 520−523.
(43) Su, Z.; Huang, J.; Shan, W.; Yan, X.-Y.; Zhang, R.; Liu, T.; Liu, Y.; Guo, Q.-Y.; Bian, F.; Miao, X.; Huang, M.; Cheng, S. Z. D. Constituent Isomerism-Induced Quasicrystal and Frank−Kasper σ Superlattices Based on Nanosized Shape Amphiphiles. *CCS Chem.* **2021**, *3*, 1434−1444.
(44) Lachmayr, K. K.; Wentz, C. M.; Sita, L. R. An Exceptionally Stable and Scalable Sugar−Polyolefin Frank−Kasper A15 Phase. *Angew. Chem., Int. Ed.* **2020**, *59*, 1521−1526.
(45) Jayaraman, A.; Zhang, D. Y.; Dewing, B. L.; Mahanthappa, M. K. Path-Dependent Preparation of Complex Micelle Packings of a Hydrated Diblock Oligomer. *ACS Cent. Sci.* **2019**, *5*, 619−628.
(46) Yue, K.; Huang, M.; Marson, R. L.; He, J.; Huang, J.; Zhou, Z.; Wang, J.; Liu, C.; Yan, X.; Wu, K.; Guo, Z.; Liu, H.; Zhang, W.; Ni, P.; Wesdemiotis, C.; Zhang, W.-B.; Glotzer, S. C.; Cheng, S. Z. D. Geometry induced sequence of nanoscale Frank-Kasper and quasicrystal mesophases in giant surfactants. *Proc. Natl. Acad. Sci. U. S. A.* **2016**, *113*, 14195−14200.
(47) Huang, M.; Hsu, C.-H.; Wang, J.; Mei, S.; Dong, X.; Li, Y.; Li, M.; Liu, H.; Zhang, W.; Aida, T.; Zhang, W.-B.; Yue, K.; Cheng, S. Z. D. Selective assemblies of giant tetrahedra via precisely controlled positional interactions. *Science* **2015**, *348*, 424−428.
(48) Su, Z.; Hsu, C.-h.; Gong, Z.; Feng, X.; Huang, J.; Zhang, R.; Wang, Y.; Mao, J.; Wesdemiotis, C.; Li, T.; Seifert, S.; Zhang, W.; Aida, T.; Huang, M.; Cheng, S. Z. D. Identification of a Frank-Kasper Z phase from shape amphiphile self-assembly. *Nat. Chem.* **2019**, *11*, 899−905.
(49) Yan, X.-Y.; Guo, Q.-Y.; Liu, X.-Y.; Wang, Y.; Wang, J.; Su, Z.; Huang, J.; Bian, F.; Lin, H.; Huang, M.; Lin, Z.; Liu, T.; Liu, Y.; Cheng, S. Z. D. Superlattice Engineering with Chemically Precise Molecular Building Blocks. *J. Am. Chem. Soc.* **2021**, *143*, 21613−21621.
(50) Baez-Cotto, C. M.; Mahanthappa, M. K. Micellar Mimicry of Intermetallic C14 and C15 Laves Phases by Aqueous Lyotropic Self-Assembly. *ACS Nano* **2018**, *12*, 3226−3234.
(51) Ungar, G.; Zeng, X. Frank-Kasper, quasicrystalline and related phases in liquid crystals. *Soft Matter* **2005**, *1*, 95−106.
(52) Nouri, B.; Chen, C.-Y.; Huang, Y.-s.; Mansel, B. W.; Chen, H.-L. Emergence of a Metastable Laves C14 Phase of Block Copolymer Micelle Bearing a Glassy Core. *Macromolecules* **2021**, *54*, 9195−9203.
(53) Yamamoto, K.; Takagi, H. Frank-Kasper and A-15 phases formed in symmetry and asymmetry block copolymer blend system. *Mater. Trans.* **2021**, *62*, 325−328.
(54) Cheong, G. K.; Bates, F. S.; Dorfman, K. D. Symmetry breaking in particle-forming diblock polymer/homopolymer blends. *Proc. Natl. Acad. Sci. U. S. A.* **2020**, *117*, 16764−16769.
(55) Bates, M. W.; Barbon, S. M.; Levi, A. E.; Lewis, R. M., III; Beech, H. K.; Vonk, K. M.; Zhang, C.; Fredrickson, G. H.; Hawker, C.

https://doi.org/10.1021/acs.macromol.2c01585
Macromolecules 2022, 55, 8918−8930

J.; Bates, C. M. Synthesis and Self-Assembly of ABn Miktoarm Star Polymers. *ACS Macro Lett.* **2020**, *9*, 396−403.
(56) Xie, N.; Li, W.; Qiu, F.; Shi, A.-C. σ Phase Formed in Conformationally Asymmetric AB-Type Block Copolymers. *ACS Macro Lett.* **2014**, *3*, 906−910.
(57) Bates, M. W.; Lequieu, J.; Barbon, S. M.; Lewis, R. M., III; Delaney, K. T.; Anastasaki, A.; Hawker, C. J.; Fredrickson, G. H.; Bates, C. M. Stability of the A15 phase in diblock copolymer melts. *Proc. Natl. Acad. Sci. U. S. A.* **2019**, *116*, 13194−13199.
(58) Mueller, A. J.; Lindsay, A. P.; Jayaraman, A.; Lodge, T. P.; Mahanthappa, M. K.; Bates, F. S. Emergence of a C15 Laves Phase in Diblock Polymer/Homopolymer Blends. *ACS Macro Lett.* **2020**, *9*, 576−582.
(59) Chen, W. C.; Liu, Y. T.; Kuo, S. W. Mesoporous Organic/Inorganic Hybrid Materials with Frank-Kasper Phases Templated by an Unusual Linear Symmetry Diblock Copolymer. *Macromol. Rapid Commun.* **2021**, No. e2100302.
(60) Hung, W.-S.; Ahmed, M. M. M.; Mohamed, M. G.; Kuo, S. W. Competing Hydrogen Bonding Produces Mesoporous/Macroporous Carbons Templated by a High-Molecular-Weight Poly (caprolactone−b−ethylene oxide−b−caprolactone) Triblock Copolymer. *J. Polym. Res.* **2020**, *27*, 173.
(61) Chu, W.-C.; Bastakoti, B. P.; Kaneti, Y. V.; Li, J.-G.; Alamri, H. R.; Alothman, Z. A.; Yamauchi, Y.; Kuo, S.-W. Tailored design of bicontinuous gyroid mesoporous carbon and nitrogen-doped carbon from poly(ethylene oxide-b-caprolactone) diblock copolymers. *Chem. − Eur. J.* **2017**, *23*, 13734−13741.
(62) Li, J.-G.; Lin, Y.-D.; Kuo, S.-W. From microphase separation to self-organized mesoporous phenolic resin through competitive hydrogen bonding with double-crystalline diblock copolymers of poly(ethylene oxide-b-ε-caprolactone). *Macromolecules* **2011**, *44*, 9295−9309.
(63) El-Mahdy, A. F. M.; Liu, T.-E.; Kuo, S.-W. Direct synthesis of nitrogen-doped mesoporous carbons from triazine-functionalized resol for CO_2 uptake and highly efficient removal of dyes. *J. Hazard. Mater.* **2020**, *391*, No. 122163.
(64) Su, W.-C.; Tsai, F.-C.; Huang, C.-F.; Dai, L.; Kuo, S.-W. Flexible epoxy resins formed by blending with the diblock copolymer PEO-*b*-PCL and using a hydrogen-bonding benzoxazine as the curing agent. *Polymer* **2019**, *11*, 201.
(65) Li, J. G.; Ho, Y. F.; Ahmed, M. M. M.; Liang, H. C.; Kuo, S. W. Mesoporous carbons templated by PEO-PCL block copolymers as electrode materials for supercapacitors. *Chem. − Eur. J.* **2019**, *25*, 10456−10463.
(66) Tsai, C.-C.; Gan, Z.; Chen, T.; Kuo, S.-W. Competitive hydrogen bonding interactions influence the secondary and hierarchical self-assembled structures of polypeptide-based triblock copolymers. *Macromolecules* **2018**, *51*, 3017−3029.
(67) Tsai, C.-C.; Gan, Z.; Kuo, S.-W. Using benzoxazine chemistry and bio-based triblock copolymer to prepare functional porous polypeptide capable of efficient dye adsorption. *Polym. Chem.* **2018**, *9*, 3684−3693.
(68) Chen, W.-C.; Liu, Y.-T.; Kuo, S.-W. Highly Thermal Stable Phenolic Resin Based on Double-Decker-Shaped POSS Nanocomposites for Supercapacitors. *Polymer* **2020**, *12*, 2151.
(69) Kuo, S.-W.*Hydrogen Bonding in Polymeric Materials*; Wiley-VCH, 2018, DOI: 10.1002/9783527804276.
(70) Kuo, S.-W.; Lin, C.-L.; Chang, F.-C. Phase behavior and hydrogen bonding in ternary polymer blends of phenolic resin/poly (ethylene oxide)/poly (ε-caprolactone). *Macromolecules* **2002**, *35*, 278−285.
(71) Kuo, S.-W. Hydrogen bonding interactions in polymer/polyhedral oligomeric silsesquioxane nanomaterials. *J. Polym. Res.* **2022**, *29*, 69.
(72) Xu, Z.; Zheng, S. Reaction-induced microphase separation in epoxy thermosets containing poly (ε-caprolactone)-block-poly (n-butyl acrylate) diblock copolymer. *Macromolecules* **2007**, *40*, 2548.
(73) Yu, R.; Zheng, S.; Li, X.; Wang, J. Reaction-induced microphase separation in epoxy thermosets containing block copolymers composed of polystyrene and poly (ε-caprolactone): Influence of copolymer architectures on formation of nanophases. *Macromolecules* **2012**, *45*, 9155.
(74) Hu, D.; Zheng, S. Reaction-induced microphase separation in epoxy resin containing polystyrene-block-poly (ethylene oxide) alternating multiblock copolymer. *Eur. Polym. J.* **2009**, *45*, 3326.
(75) Mijovic, J.; Shen, M.; Sy, J. W.; Mondragon, I. Dynamics and morphology in nanostructured thermoset network/block copolymer blends during network formation. *Macromolecules* **2000**, *33*, 5235.
(76) Tsai, S.-C.; Lin, Y.-C.; Lin, E.-L.; Chiang, Y.-W.; Kuo, S.-W. Hydrogen bonding strength effect on self-assembly supramolecular structures of diblock copolymer/homopolymer blends. *Polym. Chem.* **2016**, *7*, 2395−2409.
(77) Yu, C. Y.; Kuo, S. W. Phenolic Functionality of Polyhedral Oligomeric Silsesquioxane Nanoparticles Affects Self-Assembly Supramolecular Structures of Block Copolymer Hybrid Complexes. *Ind. Eng. Chem. Res.* **2018**, *57*, 2546−2559.
(78) Liu, C.-C.; Chu, W.-C.; Li, J.-G.; Kuo, S.-W. Mediated Competitive Hydrogen Bonding Form Mesoporous Phenolic Resins Templated by Poly(ethylene oxide-b-ε-caprolactone-b-l-lactide) Triblock Copolymers. *Macromolecules* **2014**, *47*, 6389−6400.
(79) Huang, N.; Imam, M. R.; Sienkowska, M. J.; Peterca, M.; Holerca, M. N.; Wilson, D. A.; Rosen, B. M.; Partridge, B. E.; Xiao, Q.; Percec, V. Supramolecular spheres assembled from covalent and supramolecular dendritic crowns dictate the supramolecular orientational memory effect mediated by Frank−Kasper phases. *Giant* **2020**, *1*, No. 100001.
(80) Zhang, W. B.; Cheng, S. Z. D. Giant is different: Size effects and the nature of macromolecules. *Giant* **2020**, *1*, No. 100011.
(81) Sethi, G. K.; Chakraborty, S.; Zhu, C.; Schaible, E.; Villaluenga, I.; Balsara, N. P. Effect of crystallization of the polyhedral oligomeric silsesquioxane block on self-assembly in hybrid organic-inorganic block copolymers with salt. *Giant* **2021**, *6*, No. 100055.
(82) Shao, Y.; Han, D.; Yan, X.; Hou, B.; Li, Y.; He, J.; Fu, Q.; Zhang, W. B. Phase Behaviors of Multi-tailed B_2AB_2-Type Regioisomeric Giant Surfactants at the Columnar-Spherical Boundary. *Chin. J. Chem.* **2021**, *39*, 3261−3268.

https://doi.org/10.1021/acs.macromol.2c01585
Macromolecules 2022, 55, 8918−8930